PHYSICAL REVIEW B VOLUME 32, NUMBER 12 15 DECEMBER 1985

Theoretical study of stacking faults in silicon

M. Y. Chou, Marvin L. Cohen, and Steven G. Louie
Department of Physics, University of California, Berkeley, California 94720
and Materials and Molecular Research Division, Lawrence Berkeley Laboratory, Berkeley, California 94720
(Received 9 August 1985)

The intrinsic and extrinsic stacking faults along the [111] direction in silicon are studied within the local-density-functional approach with *ab initio* pseudopotentials using a plane-wave basis set. The stacking-fault energy is obtained from first principles and is found to be in reasonably good agreement with experimental values. Electronic defect states are found within the energy gap. The defect state with energy 0.1 eV above the valence-band maximum is consistent with photoluminescence data. The electron density near the fault is found to deviate only slightly from the perfect crystal. The Hellmann-Feynman force theorem is used to study the forces on atoms near the fault and to determine the resulting structural relaxations. It is found that the interplanar separations increase by about 1% to achieve vanishing forces. This relaxation does not affect appreciably the stacking-fault energy, the eigenvalues, and other electronic properties.

I. INTRODUCTION

The study of the electronic and structural properties of defects in semiconductors has attracted considerable attention since the 1950's. Most studies concentrate on bond-breaking defects such as dislocations and vacancies. In contrast, there are few investigations of stacking faults because of the experimental and calculational difficulties resulting from the small energies involved.

Stacking faults correspond to errors in the stacking patterns without breaking any bonds. In diamond-type crystals like Si and Ge, they are often found to be accompanied by other defects. For example, dislocations (which are line defects) in Si and Ge tend to dissociate into partials and create stacking faults in between; these were observed by Ray and Cockayne[1] using weak-beam electron microscopy. One can measure the separations of these partial dislocations and deduce the stacking-fault energies from elasticity theory.[2] Several workers have performed these measurements subsequently on different types of dislocations.[2-7] The stacking-fault energies obtained were of the order of 50 erg/cm^2. This is an extremely small energy difference, since 1 erg/cm^2 is approximately equal to 6×10^{-5} eV/Å^2. Hence it is difficult to calculate the stacking-fault energies, however a calculation of this kind can serve as a crucial test of the accuracy of a theoretical approach.

Although there are several calculations[8-14] on stacking faults in silicon, to our knowledge a completely first-principles calculation has not been carried out. In the present work, we employ the density-functional formalism[15] in the local-density approximation[16] with *ab initio* norm-conserving pseudopotentials.[17] This approach has been successfully applied to many metals, semiconductors, and surface systems to obtain various structural and electronic properties.[18] In this scheme, the only input parameters are the atomic number and crystal structure. The total energies of a perfect crystal and crystals with stacking faults are calculated separately using the supercell method and a plane-wave basis set. By taking the difference between these energies, an estimate of the stacking fault energies is obtained. The resultant small energy difference is at about the limit of the precision of modern theoretical techniques within this area.

The existence of electronic energy levels within the gap is another interesting aspect associated with defects. A recent experiment by Kimerling *et al.*[19] used charge-collection scanning electron microscopy to study extrinsic stacking faults in *n*-type silicon. They suggested defect states with energies about 0.1 eV below the conduction-band minimum. More recently, Weber and Alexander,[20] using photoluminescence spectra of plastically deformed silicon, observed a stacking-fault state approximately 0.15 eV above the valence-band maximum. The possibility of defect states and other electronic properties such as the charge density of defect states will also be discussed here.

When stacking faults occur in a crystal, it is expected that the atoms near the faults relax slightly. Using the Hellmann-Feynman theorem[21] to calculate the force on each atom, we can study quantitatively the extent of this relaxation. A fully relaxed structure is obtained by using the calculated directions of the forces to indicate the motions required for a zero force reconstruction.

II. CALCULATIONS

A. Geometry

We will consider only the standard diamond structure form of silicon, and in the following sections, the terms (111) plane and [111] direction are taken with respect to the cubic fcc lattice. Along the [111] direction, the atoms follow the stacking pattern of $AA'BB'CC'AA'BB'CC'\cdots$, where the atomic layer A' (B' or C') is on top of the atomic layer A (B or C) with a separation equal to a covalent bond length. The separation between different adjacent double planes, e.g., between A' and B, is equal to one-third of a bond length.

 ©1985 The American Physical Society

Stacking faults correspond to errors in the stacking sequence with the number of tetrahedral bonds per atom unchanged. We will consider two kinds of stacking faults in this paper: the intrinsic and extrinsic stacking faults (ISF and ESF). The former can be thought of as obtained by removing a pair of atomic layers, e.g., AA', from the perfect stacking sequence, while the latter can be thought of as obtained by adding this pair of atomic layers to the perfect stacking sequence. The stacking sequence is changed to $AA'BB'CC'BB'CC'\cdots$ and $AA'BB'AA'CC'AA'BB'CC'\cdots$ for the ISF and ESF, respectively.

In order to maintain the crystal periodicity and thus many computational advantages, the supercell method is employed in this calculation. Hence the stacking faults are repeated after a certain number of atomic layers in the [111] direction, and are assumed as infinite planar defects on the (111) plane. It is required that the number of atoms per supercell by sufficiently large to avoid interactions between stacking faults, but sufficiently small to make the calculations feasible. The supercells used are hexagonal on the (111) plane with trigonal symmetry, and the third axis is along the [111] direction. Fig. 1(a) shows the projected atomic arrangement on the (111) plane. An adjacent angle of 120° is chosen for the unit vectors on this plane. When expressed in the Cartesian coordinates marked in Fig. 1(a) (the z axis is perpendicular to the page), the unit vectors are

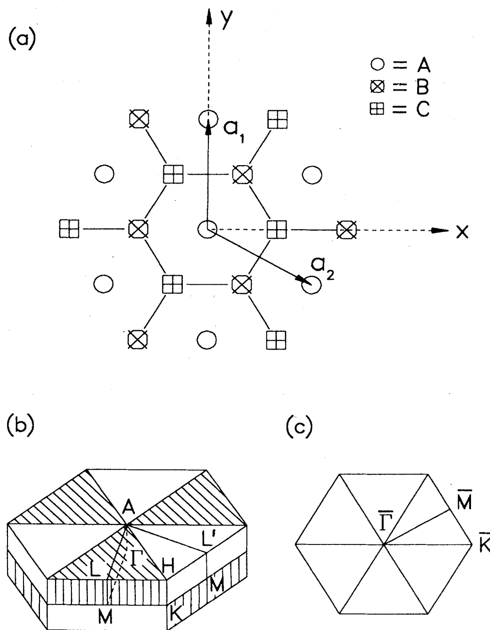

FIG. 1. (a) Projection of the atomic arrangement (see text) of silicon on the cubic (111) plane. The unit vectors for the hexagonal lattice are labeled a_1 and a_2. (b) The first Brillouin zone for this hexagonal lattice. The length in the z direction varies for different supercell lengths. The shaded parts are equivalent. (c) The two-dimensional Brillouin zone (perpendicular to the z axis).

$$\mathbf{a}_1=\frac{a_0}{2^{1/2}}\left[\frac{3^{1/2}}{2},-\frac{1}{2},0\right];\quad \mathbf{a}_2=\frac{a_0}{2^{1/2}}(0,1,0)\ ;\quad \mathbf{a}_3=n\frac{a_0}{3^{1/2}}(0,0,1)\ , \tag{1}$$

where a_0 is the cubic lattice constant and n is the number of atomic double layers in a unit cell. There are 16 atoms $AA'BB'CC'BB'CC'AA'BB'CC'$ ($n=8$) in the unit cell use for the ISF and 14 atoms $AA'BB'AA'CC'AA'BB'CC'$ ($n=7$) for the ESF. The atomic positions projected on the (111) plane (for all cases, within one unit cell) are

$$A:\ 0\mathbf{a}_1+0\mathbf{a}_2;\quad B:\ \tfrac{1}{3}\mathbf{a}_1+\tfrac{2}{3}\mathbf{a}_2;\quad C:\ \tfrac{2}{3}\mathbf{a}_1+\tfrac{1}{3}\mathbf{a}_2\ . \tag{2}$$

Both the ISF and ESF supercell structures are invariant under the symmetry operations of the space group D_{3d}^3. The hexagonal first Brillouin zone is shown in Fig. 1(b), with shaded parts being equivalent. A nonzero thickness along the z axis results from the finite size of the real space unit cell in that direction. When the length of the unit cell goes to infinity, which is the ideal case, the first Brillouin zone is reduced to a hexagon, shown in Fig. 1(c). Electronic states will be discussed later in terms of the two-dimensional Brillouin zone. In order to make a consistent comparison, the perfect crystal is also calculated in a similar unit cell with the same space group, where the smallest unit cell contains 6 atoms $AA'BB'CC'$ ($n=3$).

The ball-and-stick models for both the ISF and ESF are show in Fig. 2. For atoms near the fault plane, the numbers of first- and second-nearest neighbors, 4 and 12, respectively, are unchanged compared with the perfect crystal, but the number of third-nearest neighbors is reduced to 8 from the original value of 12. However, one additional neighboring atom is found at a distance of $5\sqrt{3}a_0/12$ ($\approx 0.722a_0$), which is only slightly larger than the second-nearest-neighbor distance $a_0/\sqrt{2}$ ($\approx 0.707a_0$). The net effect can be described as the change of the relative orientation between atoms at two ends of the sixfold rings in the diamond structure. Near the fault, the normal sixfold rings are changed to the "boatlike" arrangement, as is marked in Fig. 2.

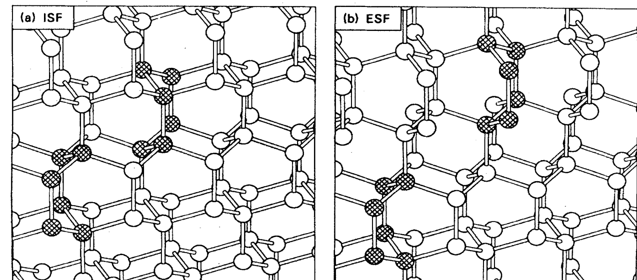

FIG. 2. Ball-and-stick models for (a) intrinsic and (b) extrinsic stacking faults. Some of the boat-shaped sixfold rings are shaded.

B. Calculational methods

To evaluate the total energy, we employ the density-functional scheme[15] in the local-density approximation.[16] The exchange-correlation energy functional used is the form suggested by Perdew and Zunger[22] based on the electron gas data by Ceperly and Alder.[23] As for the ion-electron interaction, the pseudopotential approach is employed, where the core electrons are assumed frozen (i.e., atomiclike) and only the valence electrons respond to the change of environment. These ionic pseudopotentials are norm conserving and angular momentum dependent, and are generated from free atoms.[17]

The one-particle Kohn-Sham equations are solved self-consistently using a plane-wave basis set, and the total energy is calculated in the momentum-space representation.[24] Plane waves with energies up to 10 Ry are included in the calculation. This corresponds to about 70 plane waves per atom. Stacking-fault energies are obtained by comparing the total energy of the perfect crystal and those of the crystal with stacking faults. Although neither of the two absolute energies is accurate to the order of the stacking-fault energy, the subtraction is expected to cancel most of the inherent errors since both energies are evaluated in an equivalent way. The convergence of stacking-fault energies with respect to the number of plane waves will be discussed in the next section.

Since the energy difference considered is extremely small, care must be taken to maximize accuracy. An important consideration is the summation over the Brillouin zone using a finite-k point sampling in the calculation of band energies, charge density, etc. Because the number of atomic layers per unit cell is different in each case, the k-point grid along the z direction has to be chosen accordingly. This is to ensure that each k point represents an equivalent part of k space for different structures in which the total energies are to be compared. The grid in the xy plane is chosen to be the same. We used 16 k points in the irreducible zone for both the ISF and ESF, and the total energy is compared with that of the reference perfect crystal evaluated with 26 and 36 k points, respectively.

To study the relaxation of atoms near the fault plane, we used the Hellman-Feynman theorem[21] to evaluate forces on each atom. The force acting on a specific atom is obtained by taking the explicit derivative of the total energy with respect to the basis vector of that atom;[25] the contribution from the implicit derivatives of the wave functions has been shown to vanish.[21]

III. RESULTS AND DISCUSSIONS

As a test of the numerical method, we studied the structural properties of the perfect silicon crystal in the geometry of the hexagonal six-atom unit cell. Results of the cubic lattice constant, bulk modulus, and cohesive energy[26] are listed in Table I. They are consistent with the previous calculation using the same theoretical methods[27] and are in good agreement with experimental values.[28–30] The calculated cubic lattice constant 5.41 Å will be used in the studies of stacking faults.

TABLE I. Calculated structural properties compared with experimental results and the previous calculation.

	This work	Yin and Cohen[a]	Experiment
Lattice constant (Å)	5.41	5.45	5.429[b]
Cohesive energy (eV/atom)	4.76	4.84	4.63[c]
Bulk modulus (Mbar)	0.93	0.98	0.99[d]

[a]Reference 27.
[b]Reference 28 (0 K).
[c]Reference 29 (0 K).
[d]Refernce 30 (77 K).

A. Stacking-fault energies

By comparing the total energies of the perfect and faulted crystals, we obtain stacking-fault energies of 1.9 mRy per cell for the ISF and 1.5 mRy for the ESF.[31] Dividing by the area $\sqrt{3}a_0^2/4$, these correspond to 33 erg/cm^2 and 26 erg/cm^2, respectively. The stacking-fault energy of the ESF is found to be slightly smaller than that of the ISF. This may suggest a repulsive interaction between the two deformed sixfold rings; the separation of them is slightly larger in the ESF and thus lowers the mutual interaction energy. The error resulting from the finite number of plane waves and limited k-point sampling is estimated to be 20%. We have checked the convergence with respect to number of plane waves for the ISF and the result is shown in Fig. 3.

The stacking-fault energy is divided into two contributions which are listed in Table II. First, the difference in the arrangement of ionic cores (nuclei plus core electrons) raises the electrostatic energy compared with the perfect crystal. This ion-ion energy can be calculated in the background of uniformly distributed negative charge. Since the number of changes in the surroundings is the same up to the third-nearest neighbors for both intrinsic and extrinsic stacking faults, these energies should be similar.

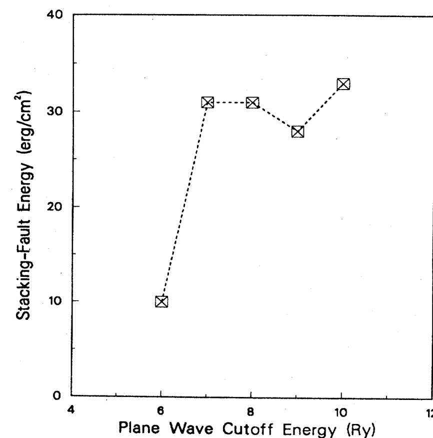

FIG. 3. Stacking-fault energy of the ISF with respect to the plane-wave energy cutoff.

TABLE II. List of various contributions to the calculated stacking-fault energies.

Energy (erg/cm^2)	ISF	ESF
Ion-ion	850	849
Electronic	−817	−823
Total	33 (±20%)	26 (±20%)

The results are 850 and 849 erg/cm^2 for the ISF and ESF, respectively. These energies are surprisingly large compared with those in the simple nonalkali metals.[13] Second, the electron distribution is altered and therefore the total electronic energy, which includes the interaction energies with the ionic cores and among themselves. This term is calculated from the local-density-functional formalism. In the cases of the stacking faults, the electronic energy is lowered and gives rise to negative differences in Table II. This effect arises mainly from the existence of one additional atom at a distance slightly farther than the second-nearest-neighbor separation. The electron-ion interaction energy is more negative and the increase in the Hartree energy is not sufficiently large to compensate the reduction. This electronic energy has to be evaluated accurately because of the large cancellation with the ion-ion energy.

In Table III, we compare this work with previous calculations and experimental values. As discussed earlier, stacking faults in real crystals are usually bounded by partial dislocations, hence the quantities measured are separations of isolated partial dislocations,[1,2,4,6,7] radii of curvature in extended nodes of dislocation networks,[2,3] or the widths of double ribbons[6] (ribbons of intrinsic and extrinsic stacking faults lying next to each other). Using the weak-beam method of electron microscopy,[1] one can image dislocations as narrow peaks and greatly increase the resolution. The experimental numbers for the stacking-fault energies are then derived from continuum elasticity theory in each case, and may be influenced by the type of defects used. These values, in erg/cm^2, vary from 50 to 70,[1–7,32] with the average deviations of measurements to be 10–20 %. In addition, the shear modulus of silicon is needed in the derivation; the suggested values can differ by 20% in the literature.[33] There are also inherent errors in treating materials with directional bonds as continuum media. Considering the uncertainties in both experiment and calculation, the agreement is satisfactory.

The ratio of the intrinsic and extrinsic stacking fault energies is also interesting. It is found to be 1.15±0.09 in the double-ribbon experiment.[6] This is expected to be more accurate than the absolute values because it is measured on one sample and is not influenced by the usual systematic uncertainties. The ratio of our calculated stacking-fault energies, 1.3, is consistent with this experimental value.

The stacking-fault energies of silicon have been studied using several theoretical approaches. They were estimated to be 44 erg/cm^2 for both the ISF and ESF by a valence force field which went beyond the harmonic approximation.[12] Chen and Falicov[8] applied a local empirical pseudopotential in second-order perturbation theory for intrinsic stacking faults. They obtained a stacking-fault energy of 55 erg/cm^2, in remarkably good agreement with experiment. Weigel and co-workers[9] calculated the stacking-fault energies by summing the band energies in the semiempirical extended Hückel theory (EHT). Their results were 86 and 85.5 erg/cm^2 for the ISF and ESF, respectively. They attributed possible discrepancies between experiment and calculation to the imperfectness of EHT parameters and the fact that measurements were performed for stacking-fault areas surrounded by different types of

TABLE III. Comparison of the stacking-fault energies between this work, previous calculations and experimental values. (EHT denotes the extended Hückel theory, NTB denotes the nonorthogonal tight-binding method, and GWF denotes the generalized Wannier function method.)

Energy (erg/cm^2)	ISF	ESF	Ratio
This work	33 (±20%)	26 (±20%)	1.3
Altmann *et al.*[a]	44	44	1.0
Chen and Falicov[b]	55		
Weigel *et al.*[c] (EHT)	86	85.5	1.0
Mattheiss and Patel[d] (NTB)			
Unrelaxed	110	85	1.3
Relaxed	64	44	1.5
Sanchez-Dehesa *et al.*[e] (GWF)			
Unrelaxed	190±30	90±30	2.1
Relaxed	145±30	50±30	2.9
Experiment[f]	50–70 (±10)		1.15±0.09[g]

[a]Reference 12.
[b]Reference 8.
[c]Reference 9.
[d]Reference 10.
[e]Reference 11.
[f]References 1–7.
[g]Reference 6.

dislocation lines, while in the calculation the ideal areas were infinite. Mattheiss and Patel[10] did a comprehensive study of silicon stacking faults using the nonorthogonal-tight-binding (NTB) method with a supercell geometry. The NTB parameters were fit to the bulk band-structure results of empirical nonlocal pseudopotentials[34] and interactions up to three shells of neighbors are included. They obtained 110 and 85 (64 and 44) erg/cm^2 for the ISF and ESF, respectively in the unrelaxed (relaxed) case. For the unrelaxed geometry, the stacking-fault energy was evaluated by taking the difference in the band energy. For the relaxed geometry, a short-range force-constant model[35] was used to account for an additional contribution coming from the difference between the ion-ion and electron-electron interaction energies. Sánchez-Dehesa *et al.*[11] employed the generalized Wannier function (GWF) method with a local pseudopotential. Their results are 190 and 90 (145 and 50) erg/cm^2 for the ISF and ESF, respectively, in the unrelaxed (relaxed) case. Both of the two calculations above found a rather significant relaxation energy for stacking faults. In contrast, the present calculation, which is a fully first-principles study, finds that relaxation gives rise to only minimal changes in the stacking-fault energy as will be discussed in Sec. III C.

B. Electronic properties

1. Eigenvalues

The calculated eigenvalues along symmetry axes of the two-dimensional Brillouin zone [Fig. 1(c)] for the crystal with stacking faults are compared with those of the perfect crystal to determine defect states related to the stacking faults. These defect states near the gap are indicated by dashed lines in Fig. 4. The shaded areas stand for the projected bands of the perfect crystal. In practice, because of the finite length of the supercell used in the calculation along the [111] direction, the calculated defect states may have small dispersions along that direction. The eigenvalues of these defect states are calculated at points with $k_z=0$ and points on the zone boundary $k_z=\frac{1}{2}G_3$. The dispersions are found to be extremely small; for example, the dispersions at $\bar{\Gamma}$ are within the thickness of the dashed lines.

The projected bands of the perfect crystal are determined from the eigenvalues calculated in the hexagonal unit cell. Some correspondences could be found between the fcc Brillouin zone and the two-dimensional hexagonal Brillouin zone. For instance, all the points from Γ to L in the first fcc Brillouin zone are projected onto one point $\bar{\Gamma}$ in the two-dimensional zone, and the point X is projected to $\bar{M}$. The conduction-band minimum is projected to somewhere between $\bar{\Gamma}$ and $\bar{M}$, and the gap calculated in the local-density-functional scheme is, as always, overly small compared with the observed value.

The calculated eigenvalues of the ISF and ESF are compared with those of the perfect crystal. The valence-band widths only differ by 0.01 eV, which tests the reliability of the supercell results. Near the energy gap, defect states are found near $\bar{\Gamma}$, $\bar{M}$, and $\bar{K}$ at energies below the conduction-band edge and slightly above the valence bands. At $\bar{\Gamma}$, these states are 0.1 eV above the valence

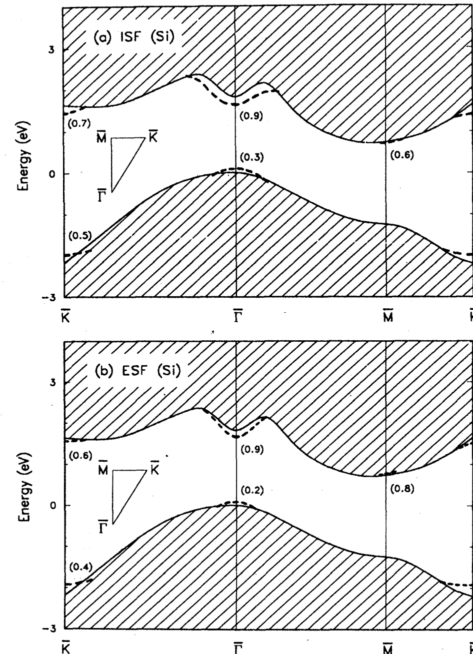

FIG. 4. Energy eigenvalues of defect states (dashed lines) in the two-dimensional Brillouin zone (perpendicular to the cubic [111] direction) for (a) ISF and (b) ESF. The valence-band maximum is chosen to be zero. The shaded area is the projected bands of the perfect crystal. Numbers in parentheses are values of the localization parameter α (see text) at $\bar{\Gamma}$, $\bar{M}$, and $\bar{K}$.

bands and 0.2 eV below the conduction bands. The former is a doubly-degenerate state above the valence-band maximum of the perfect crystal, and is occupied. This is consistent with the photoluminescence finding by Weber and Alexander.[20] On the other hand, all the states below the conduction-band edge at $\bar{\Gamma}$, $\bar{M}$, and $\bar{K}$ (with the lowest state at $\bar{M}$) are above the absolute conduction-band minimum. The positions of these states may not be determined accurately in this calculation, since the local-density-functional approximation underestimates the band gap.

Defect states found for the ISF and ESF are quite similar, as shown in Figs. 4(a) and 4(b). One of the visible differences between the ISF and ESF is that defect states of the former seem to be slightly deeper into the energy gap. All the defect states found are consistent with results of previous calculations.[10,11,14]

2. Charge density

The charge densities of the two defect states at $\bar{\Gamma}$ are plotted in Figs. 5 (ISF) and 6 (ESF). The state 0.1 eV above the valence-band maximum is shown in Figs. 5(a) and 6(a). It is an occupied state, with charge density mostly concentrated along the covalent bonds between two different pairs of atomic layers, e.g., between A' and

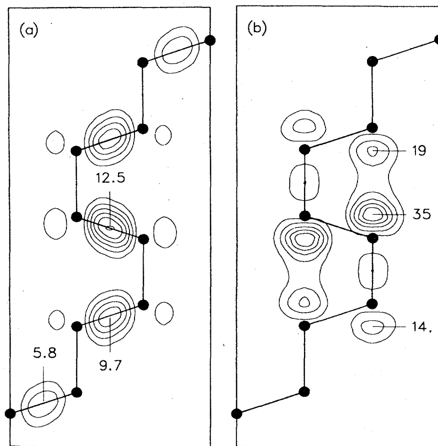

FIG. 5. Charge density of stacking-fault states at $\bar{\Gamma}$ for the ISF with energies (a) 0.1 eV above the valence-band maximum, and (b) 0.2 eV below the conduction-band edge. The charge density is in units of electrons per cell volume (cell volume=2137.07 a.u.^{3}). The plane shown is the (110) plane with contours drawn in intervals of (a) 2.0 and (b) 6.0.

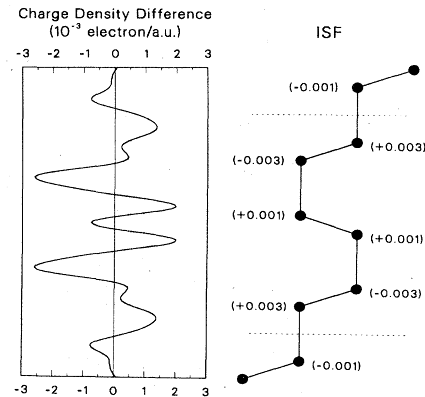

FIG. 7. Left: difference of the integrated charge density over the (111) plane between the crystal with ISF and the perfect crystal. Right: Atomic positions on the (110) plane for the ISF in the ideal geometry. Numbers in parentheses indicate the change in the net electron number associated with each atom. The region between two dashed lines is used to evaluate the localization parameter α (see text).

B. As shown in the plot, more charge density accumulates near fault atoms; the maximum is about twice higher. The charge density of the state 0.2 eV below the conduction-band edge at $\bar{\Gamma}$ is shown in Fig. 5(b) and 6(b). Almost all the charge is concentrated near the faults within the boat-shaped sixfold rings.

To examine the localization of the electron density near the fault for each electronic defect state, the electron density is integrated over a region near the fault and compared with that of a perfect crystal. A parameter α can be defined as

$$\alpha=\frac{Y-Y_0}{1-Y_0}\ , \tag{3}$$

where Y is the integrated electron density over a specific region for the ISF or ESF and Y_0 is the value for a perfect crystal. The total electron density in the unit cell is normalized to one for a single electronic state. The value of α is one if this state is fully localized within the specified region, and is zero if the integrated density is the same as that of a perfect crystal. Thus, α can be thought of as a parameter that measures the degree of localization for one state. The integration region near the fault is chosen to include three pairs of atomic layers in the case of ISF and four pairs in the case of the ESF, as indicated in Figs. 7 and 8. For defect states in the gap, the calculat-

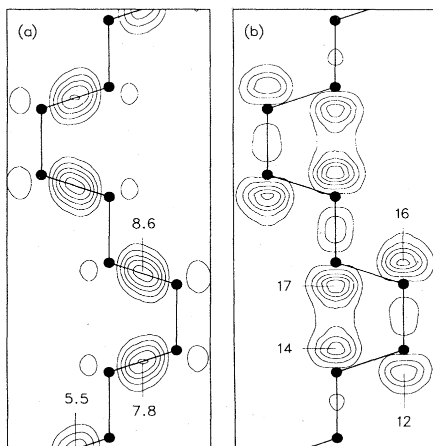

FIG. 6. Charge density of stacking-fault states at $\bar{\Gamma}$ for the ESF with energies (a) 0.1 eV above the valence-band maximum, and (b) 0.2 eV below the conduction-band edge. The charge density is in units of electrons per cell volume (cell volume=1869.94 a.u.^{3}). The plane shown is the (110) plane with contours drawn in intervals of (a) 1.5 (b) 3.0.

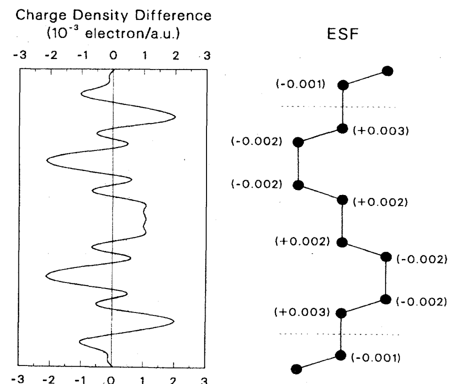

FIG. 8. Same as Fig. 7, for the crystal with ESF.

ed values of α are indicated in parentheses in Figs. 4(a) and 4(b). The unoccupied defect states near the conduction-band edge are more localized near the fault (i.e., with larger α values than the occupied states). For example, consider the two defect states at $\overline{\Gamma}$ in the ISF; α is 0.9 for the upper state and 0.3 for the occupied lower one.

It is interesting to examine how the total charge density is affected near the fault. Because the stacking sequence along the z axis has been changed, it is convenient to compare the integrated charge density over the (111) plane as a function of z. The difference in this integrated one-dimensional charge density between the faulted and perfect crystals is plotted in Fig. 7 for the ISF and in Fig. 8 for the ESF. Also shown in the same figure is the net electron number change associated with each atom. This is obtained by integrating the electron density over a slab with one atomic layer in it and subtracting from it the value of a perfect crystal with four electrons per atom. As indicated in the figures by the small unit used, the charge density changes slightly in the crystal with stacking faults. The atoms at the ends of the boat-shaped sixfold ring have slightly more electronic charge in their vicinity. However, the change is extremely small compared with those of other kinds of defects.

C. Relaxations

The calculated Hellmann-Feynman forces are displayed in Figs. 9(a) for the ISF and 10(a) for the ESF, where all the bond lengths and bond angles are the same as those in the perfect crystal. The use of the plane-wave basis set considerably reduces the computational complexity in evaluating the forces.[24,25] Since the threefold rotational symmetry around the [111] axis is maintained in the calculation, the only nonvanishing forces are along the [111] direction. These forces are orders of magnitude smaller

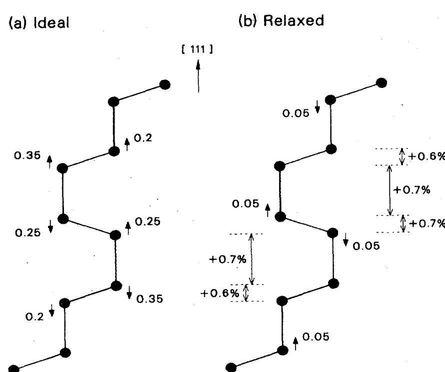

FIG. 9. Hellmann-Feynman forces on each atom in the (a) ideal and (b) relaxed geometries for the ISF. The forces are in units of 10^{-2} Ry/a.u. Arrows indicate the force directions. The atomic arrangement shown is on the (110) plane. The percentage increase of the interplanar distance is marked for the relaxed case.

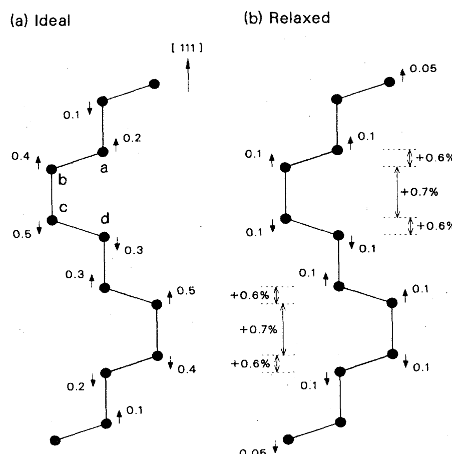

FIG. 10. Same as Fig. 9, for the crystal with ESF.

than those on ideally terminated surface atoms because of the small deviations from perfect-crystal environment. To understand how atoms tend to relax near the faults, one can get a better picture by examining the ESF case because the boat-shaped sixfold rings do not overlap. As indicated in Fig. 10(a), atoms belonging to the same double layer near the fault (atoms b and c) tend to stretch the covalent bond between them. Atoms belonging to different double layers (atoms a and d) tend to repel each other. Hence the preferred relaxation will be a stretch along the z axis with the interplanar distances near the fault increased. In the case of ISF, since the boat-shaped sixfold rings overlap slightly, the forces show a similar trend but are more complicated.

One can displace the atoms along the force direction and recalculate the new structure self-consistently. However, it is difficult to consider all of the degrees of freedom and we expect that atoms away from the fault are less relevant. Thus we consider only the relaxation of the first three interplanar separations near the fault. There are two quantities that can be examined after the displacement: the total energy of the system and the forces on each atom. We find that the slight increase in the unit-cell volume introduces much larger numerical noise for the total energy than for the forces. (This will be discussed in the Appendix.) Therefore our approach is to increase the interplanar distances near the fault and try to minimize the forces. Fig. 9(b) shows one relaxed structure for the ISF with very small residual forces. The interplanar distances near the fault are increased by 0.6—0.7 % and the forces are reduced by a factor of 5—10. Similar results for the ESF are found in Fig. 10(b). The small amount of the residual forces is close to the limit of the accuracy of the force calculation. We conclude that only a small relaxation takes place, which is estimated to be of the order of a 1% increase in the interplanar distances.

For the relaxed configurations in Figs. 9(b) and 10(b), the change of the stacking-fault energies is within the previous 20% calculational uncertainty. We do not find large relaxation energy change found in the previous cal-

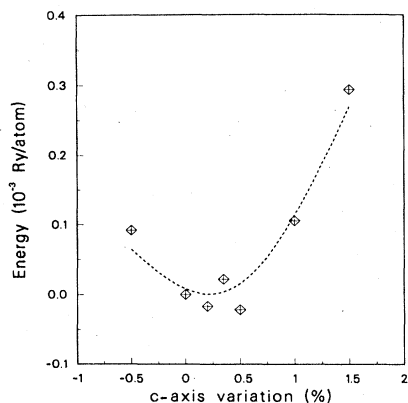

FIG. 11. Total energy change per atom with respect to c-axis variation (see Appendix) for the perfect crystal with six atoms per cell in the hexagonal lattice. The smooth dashed line is a least-squares cubic spline fit.

culations[10,11] and similarly for the eigenvalues, the difference is found to be almost negligible. Hence changes arising from the relaxation in the electronic properties can be considered to be minor.

IV. CONCLUSION

In summary, we have performed a first-principles calculation of the properties of the intrinsic and extrinsic stacking faults in silicon along the [111] direction using the local-density-functional approach with norm-conserving pseudopotentials. The calculated stacking-fault energies are in reasonably good agreement with experimental values. In particular, the ratio of the intrinsic to extrinsic stacking-fault energies agrees very well with the observed values. The small amount of energy involved in the calculation requires very high computational accuracy; it is near the limit of present theoretical techniques.

Several defect states are found with the energy-gap region in the calculation. One with energy 0.1 eV above the valence-band maximum is consistent with photoluminescence finding and consistent with some previous calculations. The charge density near the fault is also examined. Only an extremely small charge difference is found compared with the perfect crystal.

Relaxation of atoms is studied by calculating the Hellmann-Feynman forces. To minimize the forces on each atom, the interplanar distances near the fault are increased by about 1%. The change in the stacking-fault energy after relaxation is minor, and is less than the calculational uncertainty. It is found that this small relaxation does not affect the electronic properties appreciably.

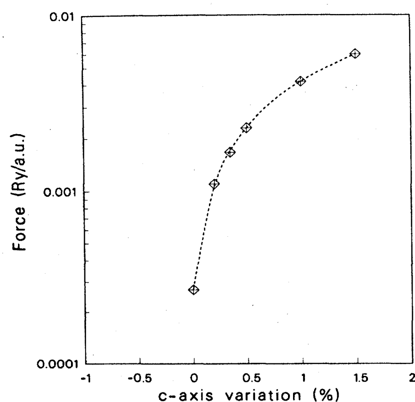

FIG. 12. Magnitude of force on each atom with respect to the c-axis variation (see Appendix) calculated for the perfect crystal with six atoms per cell in the hexagonal lattice. The smooth dashed line is a least-squares cubic-spline fit.

ACKNOWLEDGMENTS

We would to thank Dr. J. C. Phillips, Professor Eicke Weber, and Professor David Vanderbuilt for valuable discussions and comments, and Dr. S. Froyen for his help in writing the force program. We also acknowledge an IBM computer-time grant through the University of California, Berkeley. This work is supported by National Science Foundation Grant No. DMR8319024 and by the Director, Office of Energy Research, Office of Basic Energy Sciences, Material Sciences Division of the U.S. Department of Energy under Contract No. DE-AC03-76SF00098.

APPENDIX

In this appendix, we examine the calculational noise for the total energy and the forces when the unit-cell volume is slightly altered. As a test, we consider the silicon perfect crystal in the hexagonal unit cell with six atoms per cell discussed in the text. When the length scale along the c axis (the [111] direction) is uniformly expanded or compressed, it is expected that the total energy is raised and the forces on each atom increase from zero. If the volume is only changed by a very small amount, for instance, less than 0.5%, the existence of numerical noise in the total energy is expected. This is because the expected total energy change is small compared with the individual components which make up the total energy. This is within the calculational uncertainty of the absolute value of the total energy (the change of volume will affect the G-vector grid in the k space, the number of plane waves included, the interpolation of potentials, etc.). The increase in the forces on the other hand is much larger than the calculational uncertainty which is usually around 10^{-4} Ry/a.u. when full self-consistency is achieved. Figures 11 and 12, respectively, display the calculated total energy and the magnitudes of the forces with respect to small c-axis variations. The points for the total energy in Fig. 11 show appreciable fluctuations, while those for forces in Fig. 12 follow a very smooth curve in the small region of unit-cell variations. It is therefore suggested that for the small relaxations considered for the stacking faults, the use of force as a guide is more reliable than the use of total energy.

[1]I. L. F. Ray and D. J. H. Cockayne, Philos. Mag. **22**, 853 (1970).
[2]I. L. F. Ray and D. J. H. Cockayne, Proc. R. Soc. London, Ser. A **325**, 543 (1971).
[3]A. G. Cullis, J. Microsc. **98**, 191 (1973).
[4]A. Gómez, D. J. H. Cockayne, P. B. Hirsch, and V. Vitek, Philos. Mag. **31**, 105 (1975).
[5]J. C. H. Spence and H. Kolar, Philos. Mag. **30**, 59 (1979).
[6]H. Föll and C. B. Carter, Philos. Mag. A **40**, 497 (1979).
[7]H. Gottschalk, J. Phys. Paris (Colloq.) C **6**, 127 (1979).
[8]L. J. Chen and L. M. Falicov, Philos. Mag. **29**, 1 (1974).
[9]C. Weigel, H. Alexander, and J. W. Corbett, Phys. Status Solidi B **71**, 701 (1975).
[10]L. F. Mattheiss and J. R. Patel, Phys. Rev. B **23**, 5384 (1981).
[11]J. Sánchez-Dehesa, J. A. Vergés, and C. Tejedor, Phys. Rev. B **24**, 1006 (1981).
[12]S. L. Altmann, A. Lapiccirella, K. W. Lodge, and N. Tomassini, J. Phys. C **15**, 5581 (1982).
[13]C. W. Krause, Philos. Mag. **33**, 207 (1976).
[14]S. Marklund, Phys. Status Solidi B **108**, 97 (1981).
[15]P. Hohenberg and W. Kohn, Phys. Rev. **136**, B864 (1964).
[16]W. Kohn and L. J. Sham, Phys. Rev. **140**, A1133 (1965).
[17]D. R. Hamann, M. Schlüter, and C. Chiang, Phys. Rev. Lett. **43**, 1494 (1979).
[18]M. L. Cohen, Phys. Scr. T **1**, 5 (1982).
[19]L. C. Kimerling, H. J. Leamy, and J. R. Patel, Appl. Phys. Lett. **30**, 217 (1977).
[20]E. R. Weber and H. Alexander, J. Phys. Paris (Colloq.) C **4**, 319 (1983).
[21]H. Hellmann, *Einführung in die Quanten Theorie* (Deuticke, Leipzig, 1937), p. 285; R. P. Feynman, Phys. Rev. **56**, 340 (1939); J. C. Slater, J. Chem. Phys. **57**, 2389 (1972).
[22]J. P. Perdew and A. Zunger, Phys. Rev. B **23**, 5048 (1981), Appendix C.
[23]D. M. Ceperly and B. J. Alder, Phys. Rev. Lett. **45**, 566 (1980).
[24]J. Ihm, A. Zunger, and M. L. Cohen, J. Phys. C **12**, 4409 (1979); **13**, 3095(E) (1980).
[25]M. T. Yin and M. L. Cohen, Phys. Rev. B **26**, 3259 (1982).
[26]The cohesive energy is the difference between the crystal energy (including the zero-point vibration energy) and the total energy of the isolated pseudoatom (spin-polarization effects included).
[27]M. T. Yin and M. L. Cohen, Phys. Rev. B **26**, 568 (1982).
[28]J. Donohue, *The Structures of Elements* (Wiley, New York, 1974), corrected for thermal expansion and atmospheric pressure compression.
[29]L. Brewer (unpublished).
[30]H. J. McSkimin, J. Appl. Phys. **24**, 988 (1953); H. J. McSkimin and P. Andreatch, Jr., *ibid.* **34**, 651 (1963); **35**, 2161 (1964).
[31]These are small energy differences compared with those obtained from the frozen-phonon calculation for silicon. In Ref. 25, the atomic displacement employed range from 0.01 to 0.1 Å. For the LTO mode at Γ, these correspond to energy differences of 0.1 to 10 mRy per atom.
[32]See table in Ref. 6, p. 507.
[33]For example, the shear modulus used was 7.9×10^{11} dyne/cm^2 in Refs. 1–3, and 6.36×10^{11} dyne/cm^2 in Ref. 6.
[34]J. R. Chelikowsky and M. L. Cohen, Phys. Rev. B **10**, 5095 (1974).
[35]D. J. Chadi, Phys. Rev. B **19**, 2074 (1979).